In-situ analytical study of bricks exposed to marine environment using Hand-Held X-ray fluorescence spectrometry and related laboratory techniques

Héctor Morillas[a*], Cristina García-Florentino[a], Iker Marcaida[a], Maite Maguregui[b], Gorka Arana[a], Luis F.O. Silva[c] and Juan Manuel Madariaga[a]

[a]Department of Analytical Chemistry, Faculty of Science and Technology, University of the Basque Country UPV/EHU, P.O. Box 644, 48080 Bilbao, Basque Country, Spain
e-mail: hector.morillas@ehu.es
[b]Department of Analytical Chemistry, Faculty of Pharmacy, University of the Basque Country UPV/EHU, P.O. Box 450, 01080 Vitoria-Gasteiz, Basque Country, Spain
[c]Research Group in Environmental Management and Sustainability, Faculty of Environmental Sciences, Universidad De La Costa, Calle 58 #55-66, 080002 Barranquilla, Atlántico, Colombia

ABSTRACT

In this work, the degradation processes that take place in bricks exposed to marine environments have been studied. Taking into account the importance of this building material where the silicates present in the final product act as stabilizer in the porous material itself, it is necessary to understand the decay processes that occur in these aggressive environments. As is known, the marine aerosol carries different types of salts, such as chlorides, sulfates, nitrates, etc., present in surrounding environment exerting a negative influence on the materials producing cracking and disintegration processes of the material and consequently loss of brick wall stability. Nowadays the development of portable devices is taking much more importance helping researchers to resolve problems in the field in a fast and easy way. In order to extract fast and satisfactory results about the conservation state of different bricks from Punta Begoña Galleries (Getxo, Basque Country, Spain), an in-situ analytical methodology was developed based on the use of hand-held Energy Dispersive X-ray fluorescence spectrometry (HH-ED-XRF) assisted with other laboratory techniques (μ-ED-XRF and X-Ray Diffraction) in order to corroborate and complement the information obtained in-situ. This construction undergoes the influence of marine aerosol, industrial port, power generation plants, and a fuel refinery among others. The pathologies visually observable in these bricks are disintegration, breakup and detachment of the bricks. The presence of deterioration compounds in the bricks has been studied according to the orientations of the bricks inside the construction.

1. Introduction

Since ancient times, bricks are some of the most used materials in constructions. In 5,000 BC, the brick appeared as building material, and around 3,500 BC, the fired brick was finally created. Thanks to the industrialization in the 19th century, the use of brick as building material increased and acquired great importance, being one of the most used material for the building constructions [1].

Bricks used for constructions are made from clay, which is kneaded with 20-25% water. The resulting paste is molded and the bricks obtained are dried in the air [2]. Although several processes of bricks production exist, various mixtures of raw clays (mainly composed of illite-chlorite, quartz, calcite and/or dolomite, sodium and potassium feldspars, and iron oxides/hydroxides) are fired at about 900–1025°C in order to obtain the final brick [3]. Their characteristic reddish-orange colour, is indicative of the amount and type of iron oxides and oxyhidroxides present in the clay used for its manufacture [4]. However, other chemical elements such as Sb, Pb, Ca, Fe and traces of Cu have a key role in the reddish orange colour of the bricks [5]. In this sense, the composition and microstructure of the bricks are some of the most important characteristics to preserve their durability [6, 7]. Moreover, the clay must have a low amount of impurities and especially must have a low content of calcium carbonate to be plastic enough, and to avoid the presence of unreacted lime after firing. The presence of calcium carbonate in the bricks can cause cracks when the clay is mixed with water. For this reason, usually the clay must contain calcium carbonate in a proportion of less than 8-10%. During firing, a series of mineralogical transformations take place depending essentially on the initial composition, kiln temperature, heating grade, firing time and prevalence of oxidizing or reducing reactions [8-10] redefining the mineralogical composition and microstructure. In this way, after firing at 900-1025°C, kaolin is dissociated into silica and alumina and also into calcium and aluminum silicate. One of the critical factors in the conservation state of bricks is the content of calcium silicate that provides stability to the structure and

71 resistance to temperature changes. Consequently, the bricks fire or cooking temperature

72 is established as one of the most important steps in the bricks construction [11, 12].

73 Bricks, as all building materials, can experiment different chemical reactions that could

74 promote changes in their appearance and conservation state. Bricks can suffer the effect

75 of humidity [13,14], biocolonizations [15], the attack of atmospheric acidic gases [16],

76 infiltrations by aqueous solutions [17-19], the impact of marine aerosols [20, 21], dry and

77 wet depositions [22-24], freeze-thaw cycles [25], etc. These sources of deterioration, can

78 promote several chemical and physical problems as well as efflorescences formation [17],

79 loss of material [26], etc.

80 In the literature, there are many works that analyze bricks in order to extract conclusions

81 about their conservation state [27, 28], the provenance [29], original composition [30],

82 the brick composition influence on decay compounds [31], etc. Moreover, different

83 techniques such as X-Ray diffraction (XRD) [32], Raman spectroscopy [33, 1, 19],

84 infrared spectroscopy [34, 35], Inductively Coupled Plasma Mass Spectrometry (ICP-

85 MS) [36], Laser ablation Inductively Coupled Plasma Mass spectrometry (LA-ICP-MS)

86 combined with Instrumental Neutron Activation Analysis (INAA) and X-ray

87 fluorescence (XRF) [37], XRF [38] and Laser-induced breakdown spectroscopy (LIBS)

88 [39], have been used to carry out these types of analyses. In all these case studies, the

89 analytical instruments used were laboratory benchtop devices and there are no works that

90 use hand-held/portable instruments to analyze bricks and to evaluate their pathologies.

91 Sometimes the extraction of samples is a critical step, mainly due to sampling restrictions.

92 For this reason, the application of portable devices is taking much more importance,

93 helping researchers to carry out different in-situ analyses obtaining satisfactory results

94 without the necessity of taking samples [40-42, 18]. Example of these types of devices

95 are the hand-held Energy Dispersive X-Ray fluorescence spectrometers (HH-ED-XRF),

96 for which its use is being increased in the last years, because they are user friendly and

97 offer results in few seconds or minutes [43-45]. As a consequence of this, many

98 worldwide scientific groups are improving and developing new analytical methodologies

99 based on these kind of devices [46, 47].

100 In this work, a simple, fast and non-destructive methodology based on the use of a hand-

101 held Energy Dispersive X-ray fluorescence spectrometer (HH-ED-XRF) was applied to

102 perform a field analysis of bricks from Punta Begoña Galleries (Getxo, Basque Country,

103 Spain) which show different deterioration degrees depending mostly on their location in

104 front of the industrial port of Bilbao and diverse factories emitting atmospheric pollutants.

105 In order to confirm and complement conclusions extracted in-situ, additional analyses

106 were conducted in the laboratory using micro-ED-XRF spectrometry and X-Ray

107 diffraction (XRD) techniques.

108 **2. Experimental**

109 *2.1. Punta Begoña Galleries*

110

111 Punta Begoña Galleries are located in Getxo, close to Ereaga beach, in Biscay (Basque

112 Country, Spain). These galleries were built in 1918 by an industrial tycoon, Horacio

113 Echevarrieta [48]. It is one of the most significant construction in Biscay and Basque

114 Country of the 20th century. Nowadays, it is abandoned and it is poorly preserved (see

115 Fig. 1). The construction is composed by two galleries: the upper gallery or "Northwest

116 Gallery" (NG) and the lower gallery or "Southwest Gallery" (SG). The NG is oriented to

117 the northwest, and the SG is oriented to the southwest. All the construction is placed in

118 front of the sea; there is a beach in front of the NG and a leisure port in front of the SG,

119 together with the industrial port of Bilbao at 1-8 km and several factories (refinery, power

120 station plant of liquid hydrocarbons, and metallurgical companies), emitting acid gases

121 and metallic particles to the atmosphere, at not more than 10 km from the building. The

122 whole building is made by different materials such as concrete, ceramic, mortar, cement,

123 limestone and brick.

124 *2.2. In-situ analyses*

125

126 The in-situ analyses were carried out in both galleries by means of HH-ED-XRF. For this

127 purpose, seven areas from the Northwest Gallery (coded samples NG1-NG7) and

128 additional seven from the Southwest Gallery (coded samples SG1-SG7) were selected

129 (see Fig. 1). As can be observed in Fig. 1, bricks show a better or worse conservation state

130 depending on the orientation.

131 *2.3. Instrumentation*

132 The in-situ elemental analysis of the bricks was carried out using an XMET5100 (Oxford

133 Instruments, UK) hand-held energy dispersive X-Ray fluorescence spectrometer (HH-

134 ED-XRF). The instrument is equipped with an Rh tube working at a maximum voltage of

135 45 kV. The spot size of the emitted X-Ray beam is 9 mm. The analyzer includes a Peltier-

cooled silicon drift detector (SDD) of high resolution that is able to provide an energetic resolution of 150 eV (calculated for the Mn K_α line). The analyzer contains a PDA to control the spectrometer and also to save the spectra and semi-quantitative information. To determine the presence of the heaviest elements (Z>Ti) the voltage and current of the X-Ray tube was set at 40 kV and 15 µA respectively and the spectra were acquired during 100 seconds (real time) in order to improve the limit of detection for the identification of trace elements. Additionally, to remove the Bremsstrahlung and possible Bragg diffraction peaks, a 500 µm Al filter was used. In order to improve the detection of the lighter elements (Z<Ti), additional measurements were performed without the Al filter and at lower voltage (13 kV) and higher current (40 µA) during 70 seconds. In order to determine possible contributions from detector materials and possible contaminations of the XRF analyzer window, 20 repetitive spectra of an instrumental blank (a PTFE block) were acquired before each measurements batch. For the repetitive measurements, the same spectral conditions (voltage, current, filter and test time) as those used for the analysis of the bricks were considered. Although the software is based on the use of Fundamental Parameters quantification methods, in this work, the net counts of K_α lines of each detected element in the spectrum were considered following a normalization process. See elsewhere for further details [43]. To extract representative results, ten measurements (9 mm area each one) were performed randomly distributed on seven areas from the NG (NG1-NG7) and on additional seven from the SG (SG1-SG7). In order to evaluate the elemental composition of the bricks without extracting any sample, semi-quantitative information given by the HH-ED-XRF was avoided. Instead of that, a specific spectral data treatment based on the normalization of the net counts of each detected element was conducted [43]. For all the detected elements, net counts associated with K_α line were considered, except for Pb for which L_β line was used. Considering that Fe is a major element which showed an almost constant concentration in all the measured areas, its Fe K_α line was used to normalize the net counts of light elements (Z≤20) in the spectra. For the heaviest elements (Z ≥ 26), the net counts of their K_α lines were normalized against the net counts of the Compton line (incoherent scattering). This normalization process was done in order to correct possible matrix effects and variations in the positioning of the measuring sampling interface. In order to avoid spectral interferences between the As $K_{\alpha 1}$ and Pb $L_{\alpha 1}$ lines, $K_{\beta 1}$ (11.7 keV) and Pb $L_{\beta 1}$ (12.6 keV) lines were considered for As and Pb respectively.

169 In order to extract more conclusions, the elemental composition was also studied in the
170 laboratory by using the M4 TORNADO Energy Dispersive X-ray Fluorescence
171 spectrometer (Bruker Nano GmbH, Berlin, Germany). This instrument is equipped with
172 a micro-focus side window Rh X-ray tube powered by a low-power HV generator and
173 cooled by air. The spectral acquisitions in this work were performed at the maximum
174 voltage (50 kV) and current (600 µA) that the X-ray source allows. This equipment can
175 work using polycapillar lenses, which allow performing both single point measurements
176 down to 25 µm of lateral/spatial resolution, and Hyper Maps to determine the distribution
177 of each element detected in the collected fragments. A XFlash® silicon drift detector with
178 30 mm^2 sensitive area and energy resolution of 145 eV for Mn-K_α was used for
179 fluorescence radiation detection. In order to improve the detection of the lightest elements
180 (Z<11), filters were not used and measurements were acquired under vacuum (20 mbar).
181 The vacuum was achieved with a diaphragm pump MV 10 N VARIO-B. The live time
182 used for each single point measurement was 200 seconds. Two video-microscopes were
183 used to focus the area under study, a low magnification (1 cm^2 areas) one for the
184 exploration of the sample and a higher magnification one (1 mm^2 areas) for the final
185 focusing. In order to obtain the Hyper Maps, the K_α line of each element was used after a
186 previous elemental assignation and deconvolution of the spectral information using the
187 M4 TORNADO software (Bruker Nano GmbH, Berlin, Germany).

188 Finally, XRD analyses were performed with a powder diffractometer PANalytical X´Pert
189 PRO, equipped with a copper tube ($\lambda_{CuK\alpha media}$= 1.5418 Å, $\lambda_{CuK\alpha 1}$= 1.54060 Å, $\lambda_{CuK\alpha 2}$=
190 1.54439 Å), vertical goniometer (Bragg-Brentano geometry), programmable divergence
191 aperture, automatic interchange of samples, secondary monochromator from graphite and
192 PixCel detector. The measurement conditions were 40 kV and 40 mA, with an angular
193 range (2θ) scanned between 5 and 70°. For the data treatment of the diffractograms and
194 the identification of the present mineral phases, the specific software X`Pert HighScore
195 (PANalytical) in combination with the specific powder diffraction file database
196 (International Centre for Diffraction Data - ICDD, Pennsylvania, USA) was used.
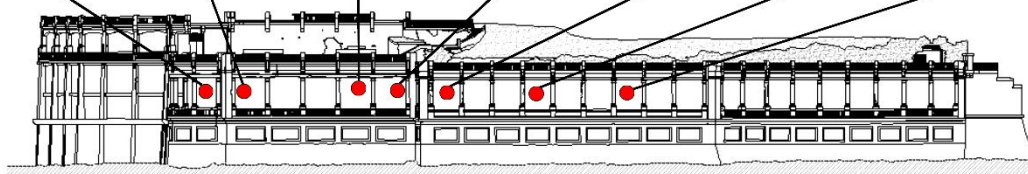
197

Punta Begoña Galleries
(Getxo, Basque Country, Spain)
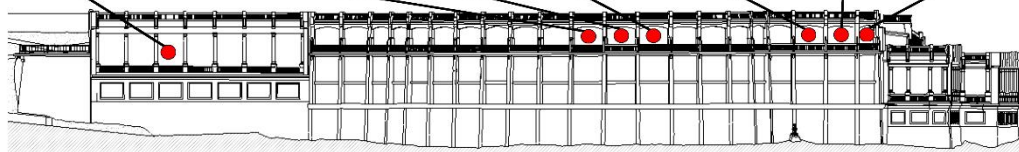
NORTH GALLERY

SOUTH GALLERY

198

Fig. 1. Punta Begoña Galleries (Getxo, Basque Country, north of Spain) and the analyzed
brick areas from their Northwest and Southwest Galleries (NG and SG).

3. Results and discussion

3.1. HH-ED-XRF analyses

To simplify the visualization of the normalized areas related to the average of the 10
spectral measurements from each studied area, they are presented as a bar graph (see Fig.
2). In Table S1 from Appendix, the normalized counts for all the elements detected in the
measured areas are presented as the average of the ten repetitive measurements on each
area together with their respective standard deviations. Among all the detected elements,
Cl, Br and Sr can be present in the brick coming from the marine aerosol [48-50]. The
last element could be also naturally present in the bricks. As it has been explained in the

7

213   experimental section, to avoid false positives the background offered by the instrument
214   (instrumental blank) was evaluated. This issue can be considered of special interest
215   considering the interference caused by the Rh Lα coming from the tube in the Cl Kα line.
216   The normalized counts of Cl, Br and Sr for all the areas in the NG and SG are quite similar
217   (see Fig. 2A), although a little bit higher values were registered in some measured areas
218   from the SG.

219   In all the analyzed areas, S was also detected. The presence of this element in the bricks
220   could suggest the possible presence of sulfates. These compounds can be present in the
221   bricks due to the influence of infiltration waters rich in sulfates or as a consequence of
222   the impact of atmospheric SO_x. Calcium carbonate that can be present on them can react
223   with the sulfates in the first case and with the H_2SO_4 coming from the atmospheric SO_x.
224   S normalized counts values are higher in the SG than in the NG, except for the case of
225   NG1 and NG7 areas.

226   Apart from elements that can be present in the bricks due to the influence of the
227   surrounding atmosphere, those related with the original composition were also evaluated.
228   In Fig. 2B, the normalized counts of these kind of elements (Al, Si, K, Ca and Fe) are
229   presented. The normalized counts of Al and Si are quite similar except for the NG7 area,
230   where a little bit higher values were registered. The presence of both elements in the
231   bricks is related with the content of silicates and aluminosilicates on them. The results
232   obtained for K are quite similar, revealing similar normalized counts values in all the
233   areas, except in the NG1 area, which shows higher values than the rest of the areas.
234   According to Ca, the highest values were registered in the SG, although in the NG high
235   values were also obtained for the NG1 and NG7 areas, as it happened for Ca. As has been
236   previously mentioned, the presence of Fe is quite similar in all the measured areas. This
237   element is related with the presence of iron oxides and oxy-hydroxides in the bricks,
238   compounds that give the characteristic orange-red color to the analyzed bricks.

239   The normalized counts of Ti, V, Cr, Mn, Ni, Cu, Zn and Pb are presented in Fig. 2C. Ti,
240   V, Cr and Mn show interference once with each other's. Thus, these interferences could
241   alter the conclusions that can be extracted analyzing the normalized counts. Leaving aside
242   this observation, the normalized counts of each element is similar in all the analyzed
243   areas, suggesting that the main contribution of these metals come from the natural raw
244   material itself. This tendency was not observed for Pb. In this case, higher normalized

245 counts were obtained in the areas from NG than in areas from SG; particularly, this
246 element was not identified in the SG2 area. This observation could suggest a possible
247 deposition of Pb coming from the surrounding atmosphere, especially in the bricks from
248 the NG area. It is necessary to remark that there are metallurgical industries from the
249 metropolitan Bilbao, not far away from the Galleries, and they contribute to emissions of
250 metallic particles, being possible their subsequent dry deposition [22, 23, 45].

251 Finally, for the rest of the detected elements (see Fig. 2D) the obtained values were similar
252 in all the measured areas except for Zr and Sn. The normalized counts of Zr are similar
253 in all the areas, except in NG7 area, where there is no presence of this element. Finally,
254 it is necessary to remark that Sn was detected in all the NG areas but only in few areas
255 from the SG was detected (SG5 and SG7)

256
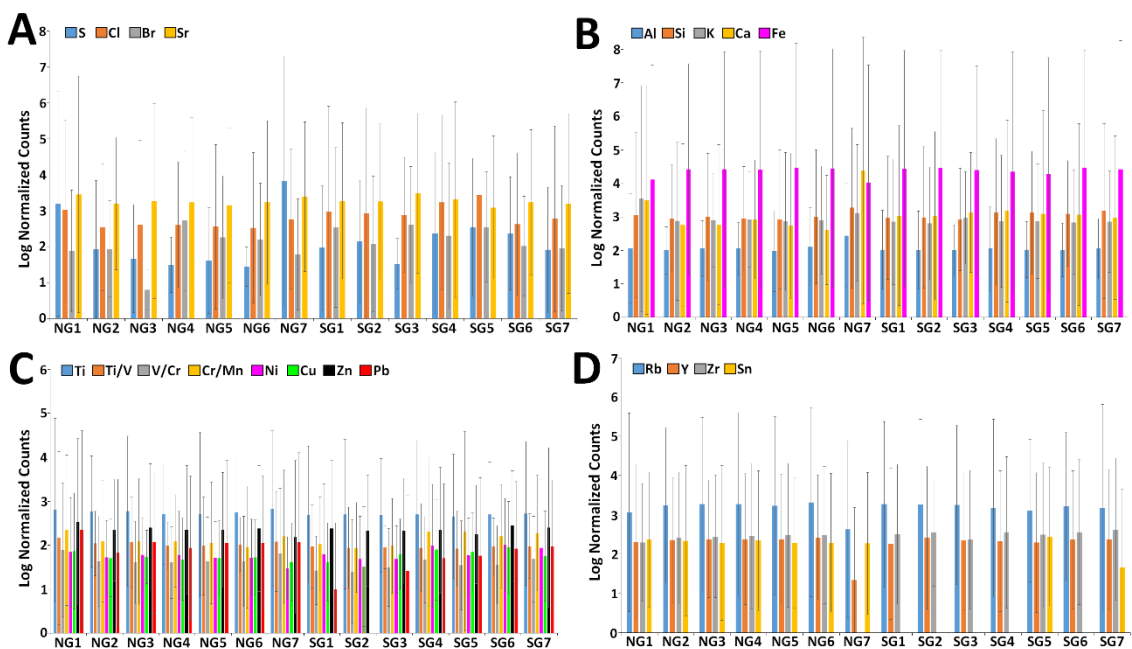
258 Fig. 2. Bar charts representing the logarithm of the normalized areas related to the average
259 of the 10 spectral measurements obtained with HH-ED-XRF on each measured area
260 together with their error bars of A) S, Cl, Br and Sr; B) Al, Si, K, Ca, Fe; C) Ti, Ni, Cu,
261 Zn, Pb and D) Rb, Y, Zr and Sn.

3.2. Principal Component Analysis (PCA) of in-situ ED-XRF results

263 In order to extract additional conclusions, the data matrix (normalized counts of NG and
264 SG areas, 14 areas x 10 analysis each) was subjected to Principal Component Analysis

265   (PCA). In this case, major elements related with the original composition of the bricks

266   such as Al, Si and Fe were removed from the data matrix before performing the PCA

267   analysis. Fig. S1 shows the scores and loadings Bi-plot. The most remarkable trend is the

268   high correlation between Ca and S (see the representation of Ca normalized counts vs. S

269   normalized counts in Fig. 3 showing a high correlation) and the high distribution of both

270   elements in NG7 area. These results confirm that this area could be the most affected one

271   by calcium sulfate salts. The formation of calcium sulfates in brick is one of the most

272   critical factors in their conservation state. According to the literature, some authors point

273   out that in some cases the formation of gypsum on the surface of the bricks material can

274   lead the inclusion and the formation of anhydrite inside the bricks as cryptoefflorescence

275   [19, 51], decreasing the stability, which is a critical factor for the bricks [52].

276   Regarding other elements, the NG1 area showed the highest values of elements such as

277   Pb, K, V/Cr, etc. Considering that the values obtained for the mentioned elements for

278   NG1 and NG7 areas are quite different, they could be considered as outlier areas with

279   respect to the rest of the measured areas that appear mixed in the scores diagram (see Fig.

280   S1 (Appendix)). In order to see additional tendencies in the rest of the areas, an additional

281   PCA was performed with the same data matrix but excluding all the measurements

282   performed in the NG1 and NG7 areas (see the scores and loadings Bi-plot in Fig. S2

283   (Appendix)). In this case, it was possible to observe how three elements highly related

284   with marine aerosol such as Cl, Br and Sr appear quite close in the loadings

285   representation. These elements, together with Ca and S (calcium sulfates?) are highly

286   related with the measurements performed in the SG. On the other hand, heavier elements

287   such as Ni, Cu, Zn, Pb, etc. are highly distributed in SG4, SG6 and SG7.

288
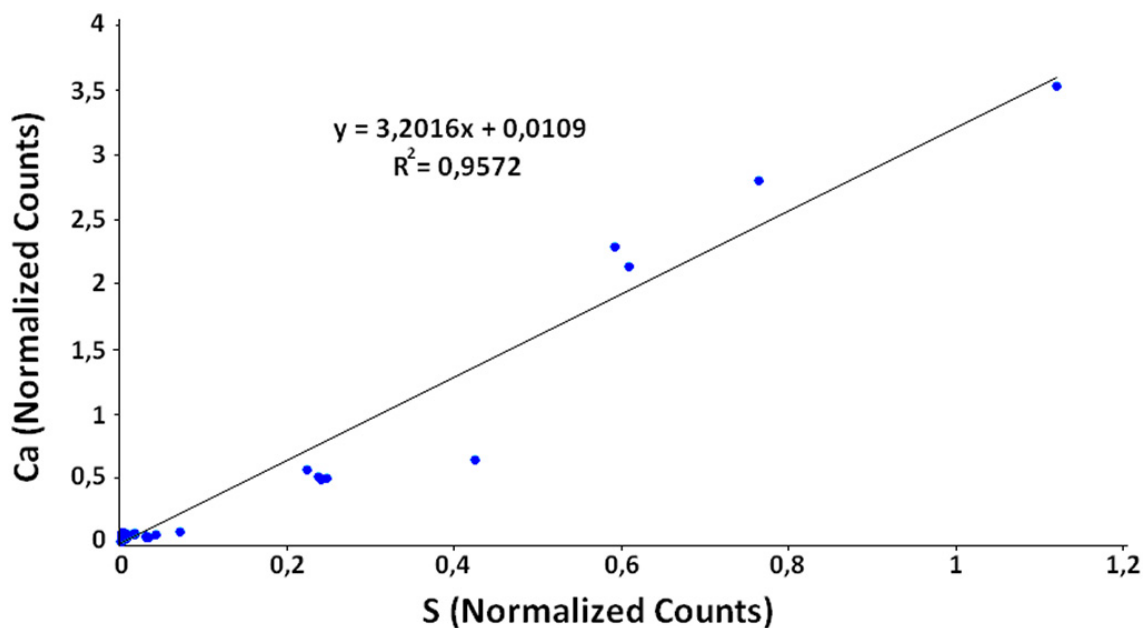
289

290   Fig. 3. Representation of Ca against S normalized counts extracted from the ten replicate

291   measurements obtained from each measured area.

3.3. μ-ED-XRF imaging of affected bricks

293   In addition to in-situ measurements, μ-ED-XRF imaging analysis was performed in order

294   to extract more conclusions about the conservation state of the bricks from Punta Begoña

295   Galleries. First of all, different single point ED-XRF spectra (spots at 1 mm of lateral

296   resolution) were acquired in the laboratory in order to confirm the presence of the

297   elements detected in-situ. In the measurements performed in the laboratory Al, Si, K Ca

298   and Fe were detected as major elements (10-60 % w/w). The concentration of Na and Cl

299   was set close to 2%, thus it can be concluded that the impact of chlorides coming from

300   marine aerosol is quite evident. Moreover, it can be concluded that calcium carbonate

301   present in the bricks as original component or as a carbonation product coming from the

302   original CaO, which suffers a hydration process and a subsequent sulfation process, since

303   the S content in the bricks was set close to 0.5%. Apart from that, Ti and Mn were also

304   present in the brick samples as minor elements (between 0.5-1%). Additional trace

305   elements (< 0.1%) were also found in the brick samples such as Mg, V, Cr, Ni, Cu, Zn,

306   Ga, Pb, Rb, Sr, Y, Zr, Br and Ba. Although Ga can be considered an unusual element in

307   bricks, it can be present in ceramic matrix at trace levels. The presence of Br in the brick

308   could not be attributed to a natural origin, thus it can be related with the marine aerosol

309   influence. Moreover, the presence of both V and Cr was also confirmed, resolving in this

310   way the uncertainty in the assignation of both elements by means of HH-ED-XRF. In the

11

311   ED-XRF spectra obtained in the laboratory, and thanks to the use of a more powerful

312   software than the one employed in the HH-ED-XRF measurements, it was possible to

313   perform a deconvolution of those XRF lines, which show interferences. In this case, it

314   was also possible to confirm the presence of Sn in the bricks from all the areas. In the in-

315   situ ED-XRF, this element was not detected in all the areas, suggesting an improvement

316   in the limit of detection for this element using the benchtop ED-XRF spectrometer.

317   After single point analyses, a fragment of one of the most damaged brick was selected

318   (NG1) in order to perform an imaging study by means of μ-ED-XRF. A section of the

319   brick was mapped in order to confirm if elements associated with marine aerosol and

320   other pollutants have penetrated to the inner areas of the brick (see Fig. 4). The size of

321   the mapped area was 7.41 (height) x 45 (width) mm and each pixel (1301956 in total,

322   16x16 μm in size/each) was acquired during 10 ms. In order to reduce the time of the

323   mapping acquisitions and considering that a good resolution was obtained, one frame

324   count (cycle) was considered. In the mapped section, a whitish accumulation or vein is

325   observable in the central part of the brick section (see Fig. 4). In the whole section of the

326   brick, (alumino) silicates are widely distributed (see Al and Si maps in Fig. 4) indicating

327   clearly its presence in the original clays used. With the imaging study, it can be confirmed

328   that Fe, a natural component of the bricks, is homogeneously distributed in the brick, as

329   it was pointed out in the in-situ HH-ED-XRF studies. Regarding the presence of metals,

330   it is evident the high correlation between Ti, V and Ni (see the coincident distribution of

331   Ti-V (pink) and Ni (green)), which are concentrated in the central vein of the brick.

332   Moreover, inclusions of Mn were also detected in the bulk of the brick.

333   The μ-ED-XRF study also revealed interesting results related with the elements present

334   in the marine aerosol. According to the Na-Cl map (pink) presented in the Fig. 4, the high

335   correlation between both element suggest that halite (NaCl) is crystalized inside the pores

336   of the bricks. The identification of this salt in the inner parts of the bricks suggest a high

337   penetration of this salt to the inner areas of the bulk material. These salt crystallizations

338   can contribute to physical stress in the brick structure promoting fissures, cracks and

339   disintegrations of the brick. The imaging study also confirms that Br is homogenously

340   distributed (see its map in light blue in Fig. 4), confirming the natural origin of Br in the

341   brick and discarding a possible input of this element coming from the marine aerosol, as

342   was proposed at the sight of HH-ED-XRF results. Finally there is also a high correlation

343   between Ca and S distribution (see Fig. 4) suggesting the presence of gypsum

344 (CaSO$_4$·2H$_2$O)/anhydrite (CaSO$_4$) in the inner parts of the bricks, confirming in this was

345 the sulfation process of the calcium carbonate of the bricks. Gypsum is more soluble than

346 calcium carbonate, accelerating in this way the dissolution and disintegration process of

347 the bricks.

348

349
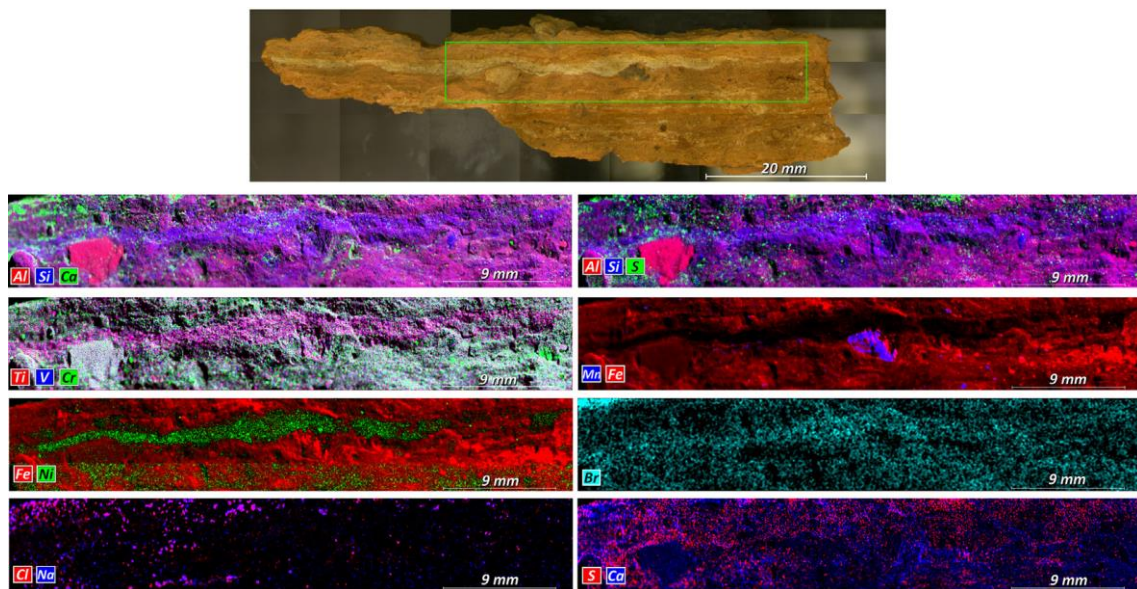
350 Fig. 4. μ-ED-XRF imaging of one of the analyzed brick observing the elemental

351 distribution of different elements.

3.4. Mineralogical composition of bricks from Punta Begoña Galleries

353 To determine the mineralogical composition of bricks samples from all the areas in the

354 Galleries, the XRD technique was used. In Table 1, the obtained results are shown. In the

355 analyzed brick samples (one sample from each area, 14 in total), the bricks mineralogy is

356 dominated by quartz (α-SiO$_2$) and phyllosilicates (micas and/or illites). In the fourteen

357 brick samples analyzed it was not possible to identify the presence of calcium silicates

358 (see Table 1). These kind of silicates (e.g. gehlenite, diopside, anortite, etc.) are to be

359 present in the bricks because they are generated during the firing of the raw material

360 (usually calcareous clays), by reaction at high temperatures between the initial silicates

361 and the released CaO in the decomposition of calcite. The absence of calcium silicates in

362 the characterized bricks suggest a high deterioration process on them, confirmed by the

363 presence of high amounts of silica, the byproduct obtained after the acidification of such

364 silicates [16]. Additionally, in bricks and ceramic materials, vitreous material is usually

13

365 present. In this case, also, it was not possible to identify this kind of material in the bricks
366 from Punta Begoña Galleries.

367 Apart from the mentioned major compounds, additional minor components were also
368 detected (see Table 1). Among them, hematite (α-Fe_2O_3) responsible of the orange-red
369 color of the bricks was identified in all the bricks. By means of XRD, it was not possible
370 to detect the presence of iron oxi-hydroxides, which does not mean that they are not
371 present in the bricks. These compounds can be present at lower concentrations, being
372 impossible to detect them by XRD. Apart from the expected phyllosilicates, which are
373 present as major components of the bricks, in one of the bricks (NG1), phyllosilicates of
374 the chlorite group were also identified.

375 Regarding the deterioration compounds in the bricks, halite (NaCl) was detected in all the
376 bricks, confirming the influence of marine aerosol. Apart from that, calcite, high
377 magnesium calcite (HMC) and gypsum ($CaSO_4 \cdot 2H_2O$) were identified. This last
378 compound was detected in three samples from the NG and in four samples from the SG.
379 As was mentioned above, sulfates cannot be considered original components of the
380 ceramic materials cooked at high temperature. Due to this reason, these types of
381 compounds can be considered as decay compounds coming from the calcite and HMC
382 present in all the bricks [16].

383
4. Conclusions

385 This work demonstrated that hand-held energy dispersive X-ray fluorescence
386 spectrometry can be used as a rapid tool to extract conclusions about the original
387 composition of bricks and possible deterioration products present on them from an
388 elemental point of view. Considering that semi-quantitative approaches offered by this
389 kind of devices cannot be considered accurate enough to extract conclusions, the best
390 option is to use the counts given for each element in order to perform a comparative study
391 between different analyzed areas. It is crucial to apply a good normalization and
392 correction step in order to avoid possible matrix effect and deviations due to the
393 positioning of the sampling interface. Following this procedure, in this study it was
394 possible to extract interesting conclusions about the deterioration process of the bricks.
395 In this sense, it was possible to determine the presence of NaCl, confirming the influence
396 of marine aerosol. Moreover, S was highly distributed in the bricks suggesting a possible

presence of sulfate salts in the bricks. Concretely, thanks to HH-ED-XRF analyses and a subsequent data treatment (PCA) we concluded that the areas most affected by sulfates were the ones of the Southwestern Gallery (SG areas). This observation was confirmed in the laboratory by XRD, since gypsum ($CaSO_4 \cdot 2H_2O$) was identified in a higher number of samples extracted from the SG areas than from the NG ones. An exception should be mentioned in the NG, specifically in the NG7 area where high values of S and Ca were determined. Moreover, HH-ED-XRF also approach the extended distribution of Ca in the bricks, which can be related with gypsum but also with the high magnesium calcite (HMC) as it was confirmed by XRD. Sometimes the clay or sand used to create the bricks contain carbonates or organic matter. During the firing process, these components behave in a different way comparing with the silicates present in the clay. The original carbonates can be decomposed into calcium oxide, which can be transformed into calcium hydroxide with the atmospheric humidity and suffer a subsequent carbonation process to give rise to the calcium carbonate. The carbonate can react with sulfates carried in infiltration waters or with the atmospheric SO_x to give rise to new sulfate salts (mainly gypsum), more soluble than the original carbonate, which can unchain the loss of material in the bricks. Moreover, the absence of calcium silicates in the bricks and the anomalous high silica abundances, suggest the high deterioration degree of these ceramic materials in the walls of the Punta Begoña Galleries.

Apart from that, HH-ED-XRF spectroscopy was useful to identify a possible deposition of metals coming from the atmosphere. Concretely, an increase of Pb presence was determined in the bricks from the NG. This observation should be confirmed in future works in order to confirm if this additional input could be considered natural or coming from anthropogenic origin.

As general conclusion it can be said that not only the atmosphere which surrounds the bricks (marine aerosol, infiltrations, SO_x influence, metallic depositions, etc.) have influence in the conservation state of the bricks from Punta Begoña Galleries. The high presence of calcium carbonate detected nowadays in the bricks, promoted probably due to the high presence of original carbonates in the original clays/sands used to create the bricks, play a crucial role in the burst of deterioration process assisted by different anthropic factors or sources.

Acknowledgements

Appendix A. Supplementary data

Supplementary data to this article can be found online at DOI:..

References

[1] M. Maguregui, A. Sarmiento, R. Escribano, I. Martinez-Arkarazo, K. Castro, J.M. Madariaga, Raman spectroscopy after accelerated ageing tests to assess the origin of some decayed products found in real historical bricks affected by urban polluted atmospheres, Anal. Bioanal. Chem. 395 (2009) 2119-2129.

[2] A. Angiolani, Introducción a la química Industrial. Fundamentos químicos y tecnológicos. Edit. Andres Bello. Santiago de Chile, Chile, 1960.

[3] A. Viani, K. Sotiriadis, A. Len, P. Šašek, R. Ševčík, Assessment of firing conditions in old Fired-clay bricks: The contribution of X-ray powder diffraction with the Rietveld method and small angle neutron scattering, Mater. Charact. 116 (2016) 33-43.

[4] R. Kreimeyer, Some Notes on the Firing Color of Clay Bricks, Appl. Clay Sci. 2 (1987) 175-183.

456 [5] P. Holakooei, A multi-spectroscopic approach to the characterization of early glaze
457 opacifiers: Studies on an Achaemenid glazed brick found at Susa, south-western Iran
458 (mid-first millennium BC), Spectrochim. Acta A 116 (2013) 49-56.

459 [6] G. Cultrone, I. Sidraba, E. Sebastián, Mineralogical and physical characterization of
460 the bricks used in the construction of the "Triangul bastion", Riga (Latvia), Appl.Clay
461 Sci. 28 (2005) 297–308.

462 [7] K. Elert, G. Cultrone, C. Rodriguez Navarro, E. Sebastián, Durability of bricks used
463 in the conservation of historic buildings—influence of composition and microstructure,
464 J. Cult. Herit. 4 (2003) 91–99.

465 [8] R. Fort, M. Alvarez de Buergo, M.C. López de Azcona, F. Mingarro, M.J. Varas, J.
466 Soriano, Caracterización de la Fábrica de Ladrillo del Palacio del Infante Don Luis,
467 Boadilla del Monte, Madrid, Bol. Soc. Esp. Ceram. Vidrio 43 (2004) 578-582.

468 [9] M. Maggetti, Phase Analysis and its Significance for Technology and Origin, J.S.
469 Olin, A.D. Franklin (Eds.), Archaeological Ceramics, Smithsonian Institution Press,
470 Washington D.C (1982), pp. 121-133.

471 [10] L. Maritan, L. Nodari, C. Mazzoli, A. Milano, U. Russo, Influence of firing
472 conditions on ceramic products: experimental study on clay rich in organic matter, Appl.
473 Clay Sci. 31 (2006) 1-15.

474 [11] B. Bauluz, M.J. Mayayo, A. Yuste, C. Fernandez-Nieto, J.M. Gonzalez Lopez, TEM
475 study of mineral transformations in fired carbonated clays: relevance to brick making,
476 Clay Miner. 39 (2004) 333–344.

477 [12] G. Cultrone, E. Sebastián, K. Elert, M.J. de la Torre, O. Cazalla, C. Rodriguez-
478 Navarro, Influence of mineralogy and firing temperature on the porosity of bricks, J. Eur.
479 Ceram. Soc. 24 (2004) 547–564.

480 [13] H. Morillas, M. Maguregui, O. Gómez-Laserna, J. Trebolazabala, J.M. Madariaga,
481 Characterisation and diagnosis of the conservation state of cementitious materials
482 exposed to the open air in XIX century lighthouses located on the coast of the Basque
483 Country: The case of Igueldo lighthouse, San Sebastian, North of Spain, J. Raman
484 Spectrosc. 43 (2012) 1630-1636.

485   [14] H. Morillas, M. Maguregui, O. Gómez-Laserna, J. Trebolazabala, J.M. Madariaga,

486   Could marine aerosol contribute to deteriorate building materials from interior areas of

487   lighthouses? An answer from the analytical chemistry point of view, J. Raman Spectrosc.

488   44 (2013) 1700–1710.

489   [15] H. Morillas, M. Maguregui, I. Marcaida, J. Trebolazabala, I. Salcedo, J.M.

490   Madariaga, Characterization of the main colonizer and biogenic pigments present in the

491   red biofilm from La Galea Fortress sandstone by means of microscopic observations and

492   Raman Imaging, Microchem. J. 121 (2015) 48–55.

493   [16] A. Sarmiento, M. Maguregui, I. Martinez-Arkarazo, M. Angulo, K. Castro, M.A.

494   Olazabal, L.A. Fernandez, M.D. Rodriguez-Laso, A.M. Mujika, J. Gomez, J.M.

495   Madariaga, Raman spectroscopy as a tool to diagnose the impacts of combustion and

496   greenhouse acid gases on properties of Built Heritage, J. Raman Spectrosc. 39 (2008)

497   1042-1049.

498   [17] H. Morillas, M. Maguregui, J. Trebolazabala, J.M. Madariaga, Nature and origin of

499   white efflorescence on bricks, artificial stones and joint mortars of modern houses

500   evaluated by portable Raman spectroscopy and laboratory analyses, Spectrochim. Acta A

501   136 (2015) 1195-1203.

502   [18] H. Morillas, J. García-Galan, M. Maguregui, C. García-Florentino, I. Marcaida, J.A.

503   Carrero, J.M. Madariaga, In-situ multianalytical methodology to evaluate the

504   conservation state of the entrance arch of La Galea Fortress (Getxo, north of Spain),

505   Microchem. J. 128 (2016) 288-296.

506   [19] M. Maguregui, A. Sarmiento, I. Martínez-Arkarazo, M. Angulo, K. Castro, G. Arana,

507   N. Etxebarria, J.M. Madariaga, Analytical diagnosis methodology to evaluate nitrate

508   impact on historical building materials, Anal. Bioanal. Chem. 391 (2008) 1361–1370.

509   [20] H. Morillas, M. Maguregui, C. Paris, L. Bellot-Gurlet, P. Colomban, J.M.

510   Madariaga, The role of marine aerosol in the formation of (double) sulfate/nitrate salts in

511   plasters, Microchem. J. 123 (2015) 148-157.

512   [21] H. Morillas, J. García-Galán, M. Maguregui, I. Marcaida, C. García-Florentino, J.A.

513   Carrero, J.M. Madariaga, Assessment of marine and urban-industrial environments

514 influence on built heritage sandstone using X-ray fluorescence spectroscopy and
515 complementary techniques, Spectrochim. Acta B. 123 (2016) 76-88.

516 [22] H. Morillas, M. Maguregui, C. García-Florentino, I. Marcaida, J.M. Madariaga,
517 Study of particulate matter from Primary/Secondary Marine Aerosol and anthropogenic
518 sources collected by a self-made passive sampler for the evaluation of the dry deposition
519 impact on Built Heritage, Sci. Total Environ. 550 (2016) 285-296.

520 [23] H. Morillas, I. Marcaida, C. García-Florentino, M. Maguregui, G. Arana, J.M.
521 Madariaga, Micro-Raman and SEM-EDS analyses to evaluate the nature of salt clusters
522 present in secondary marine aerosol, Sci. Total. Environ. 615 (2018) 691-697.

523 [24] H. Morillas, I. Marcaida, M. Maguregui, J.A. Carrero, J.M. Madariaga, The influence
524 of rainwater composition on the conservation state of cementitious building materials,
525 Sci. Total Environ. 542 (2016) 716-727.

526 [25] E.M. Perez-Monserrat, F. Agua, R. Fort, M. Alvarez de Buergo, J.F. Conde, M.
527 García-Heras, Effect of manufacturing methods on the decay of ceramic materials: A case
528 study of bricks in modern architecture of Madrid (Spain), Appl. Clay Sci. 135 (2016) 136-
529 149.

530 [26] B. Lubelli, R.P.J van Hees, C.J.W.P. Groot, The role of sea salts in the occurrence
531 of different damage mechanisms and decay patterns on brick masonry, Constr. Build.
532 Mater. 18 (2004) 119-224.

533 [27] P. Aloise, M. Ricca, M.F. La Russa, S.A. Ruffolo, C.M. Belfiore, G. Padeletti, G.M.
534 Crisci, Diagnostic analysis of stone materials from underwater excavations: the case study
535 of the Roman archaeological site of Baia (Naples, Italy), Appl. Phys. A-Mater. 114 (2014)
536 655-662.

537 [28] A.A. El-Midany, H.M. Mahmoud, Mineralogical, physical and chemical
538 characteristics of historic brick-made structures, Miner. Petrol. 109 (2015) 733-739.

539 [29] L. Bonizzoni, A. Galli, M. Gondola, M. Martini, Comparison between XRF, TXRF,
540 and PXRF analyses for provenance classification of archaeological bricks, X-Ray
541 Spectrom.42 (2013) 262-267.

542 [30] J. Chen, M. Yan, J. Su, B. Li, J. Sun, The kiln coating formation mechanism of MgO-
543 $FeAl_2O_4$ brick, Ceram. Int. 42 (2016) 569-575.

544 [31] J-H. Chen, D-F. Liu, M-W. Yan, P. Jiang, B. Li, J-L. Sun, Influence of
545 Microstructure on Formation of Deterioration Layer in Periclase-Hercynite Bricks,
546 Refract. Ind. Ceram. 57 (2016) 267-272.

547 [32] S. Belgacem, H. Galai, H. Tiss, Qualitative and quantitative investigation of post-
548 mortem cement refractory: The case of magnesia-spinel bricks, Ceram. Int. 42 (2016)
549 19147-19155.

550 [33] J.M. Alia, H.G.M. Edwards, F.J. García-Navarro, J. Parras-Armenteros, C.J.
551 Sanchez-Jimenez, Application of FT-Raman spectroscopy to quality control in brick
552 clays firing process, Talanta 50 (1999) 291-298.

553 [34] V.Z. Abdrakhimov, E.S. Abdrakhimova, Phase Composition and Porosity Structure
554 of Ceramic Bricks More Than 100 Years Old: Catholic Church, Iverskiy Monastery, and
555 Church of the Nativity in Samara Oblast, Glass Ceram. 73 (2016) 111-114.

556 [35] N.A. Pérez, L. Bucio, E. Lima, E. Soto, C. Cedillo, Identification of allophane and
557 other semi-crystalline and amorphous phases on pre-Hispanic Mexican adobe earth bricks
558 from Cholula, Mexico, Microchem. J. 126 (2016) 349-358.

559 [36] D.N. Phillips, Vanadium staining in fired clay bricks, Brit. Ceram. T. 102 (2003)
560 257-260.

561 [37] N. Scheid, S. Becker, M. Duecking, G. Hampel, J. Volker Krantz, P. Watzke, P. Weis, S.
562 Zauner, Forensic investigation of brick stones using instrumental neutron activation
563 analysis (INAA), laser ablation-inductively coupled plasma-mass spectrometry (LA-ICP-
564 MS) and X-ray fluorescence analysis (XRF), Appl. Radiat. Isotopes, 67 (2009) 2128-
565 2132.

566 [38] L. Bonizzoni, ED-XRF analysis for Cultural Heritage: is quantitative evaluation
567 always essential?, J. Phys. Conf. Ser. 630 (2015) 012001/1-012001/9.

568 [39] S.S. Rai, N. K. Rai, A.K. Rai, U.C. Chattopadhyaya, Rare earth elements analysis in
569 archaeological pottery by laser induced breakdown spectroscopy, Spectroscopy Letters
570 49 (2016) 57-62.

571 [40] C. García-Florentino, M. Maguregui, H. Morillas, U. Balziskueta, A. Azkarate, G.
572 Arana, J.M. Madariaga, Portable and Raman imaging usefulness to detect decaying on

573 mortars from Punta Begoña Galleries (Getxo, North of Spain), J. Raman. Spectrosc. 47
574 (2016) 1458–1466.

575 [41] J.M. Madariaga, M. Maguregui, S. Fdez Ortiz-De Vallejuelo, U. Knuutinen, K.
576 Castro, I. Martinez-Arkarazo, A. Giakoumaki, A. Pitarch, In situ analysis with portable
577 Raman and ED-XRF spectrometers for the diagnosis of the formation of efflorescence on
578 walls and wall paintings of the Insula IX 3 (Pompeii, Italy), J. Raman Spectrosc. 45 (2014)
579 1059-1067.

580 [42] J.M. Madariaga, M. Maguregui, K. Castro, U. Knuutinen, I. Martinez-Arkarazo,
581 Portable Raman, DRIFTS, and XRF analysis to diagnose the conservation state of two
582 wall painting panels from Pompeii deposited in the Naples National Archaeological
583 Museum (Italy), App. Spectrosc. 70 (2016) 137-146.

584 [43] C. García-Florentino, M. Maguregui, H. Morillas, I. Marcaida, J.M. Madariaga, A
585 fast in situ non-invasive approach to classify mortars from a construction of high
586 historical value, Microchem. J. 133 (2017) 104-113.

587 [44] I. Marcaida, M. Maguregui, S. Fdez-Ortiz de Vallejuelo, H. Morillas, N. Prieto-
588 Taboada, M. Veneranda, K. Castro, J.M. Madariaga, In situ X-ray fluorescence-based
589 method to differentiate among red ochre pigments and yellow ochre pigments thermally
590 transformed to red pigments of wall paintings from Pompeii, Anal. Bioanal. Chem. 409
591 (2017) 3853-3860.

592 [45] H. Morillas, M. Maguregui, C. García-Florentino, J.A. Carrero, I. Salcedo, J.M.
593 Madariaga, The cauliflower-like black crusts on sandstones: A natural passive sampler to
594 evaluate the surrounding environmental pollution, Environ. Res. 147 (2016) 218-232.

595 [46] S. Pessanha, M. Alves, J.M. Sampaio, J.P. Santos, M.L. Carvalho, M. Guerra, A
596 novel portable energy dispersive X-ray fluorescence spectrometer with triaxial geometry,
597 J. Inst. 12 (2017) P01014/1-P01014/13.

598 [47] S. Pessanha, A. Samouco, R. Adão, M.L. Carvalho, J.P. Santos, P. Amaro, Detection
599 limits evaluation of a portable energy dispersive X-ray fluorescence setup using different
600 filter combinations, X-ray Spectrom. 46 (2017) 102-106.

601 [48] B. Estornés Lasa, in Horacio Echevarrieta Maruri, Auñamendi Eusko Entziklopedia,
602 Euskomedia fundazioa, Donosti, 2008.

21

603 [49] S-H. Zhang, G-P. Yang, H-H. Zhang, J. Yang, Spatial variation of biogenic sulfur in
604 the south Yellow Sea and the East China Sea during summer and its contribution to
605 atmospheric sulfate aerosol, Sci. Total. Environ. 488-489 (2016) 157-167.

606 [50] K. Ballschmiter, Pattern and sources of naturally produced organohalogens in the
607 marine environment: biogenic formation of organohalogens, Chemosphere 52 (2003)
608 313-324.

609 [51] F. Moreno, S.A.G. Vilela, A.S.G. Antunes, C.A.S. Alves, Capillary-rising salt
610 pollution and granitic stone erosive decay in the parish church of Torre de Moncorvo (NE
611 Portugal)-implications for conservation strategy, J.Cult. Herit. 7 (2006) 56-66.

612 [52] M. Maguregui, R. Tagliapietra, M. Angulo, I. Martinez-Arkarazo, K. Castro, J.M.
613 Madariaga, A. Brooker, Identification of historical bricks degradation products by means
614 of Combined Raman spectroscopy and scanning electron microscopy, in Conservation
615 Science 2007 Publisher: Archetype, UK, London, Editors: J.H. Townsend, L. Toniolo, F.
616 Capitelli, pp. 212-219.

617
618
619 **FIGURE CAPTIONS**

620

621 **Fig.1.** Punta Begoña Galleries (Getxo, Basque Country, north of Spain) and the analyzed
622 brick areas from their Northwest and Southwest Galleries.

623 **Fig.2.** Bar charts with normalized areas related to the average of the 10 spectral
624 measurements obtained with HH-ED-XRF and their error bars of A) S, Cl, Br and Sr; B)
625 Al, Si, K, Ca ,Fe ; C) Ti, Ni, Cu, Zn, Pb and D) Rb, Y, Zr and Sn.

626 **Fig.3**. Correlation graph of the Ca and S normalized counts and analyzed areas.

627 **Fig.4.** μ-ED-XRF imaging of one of the analyzed brick observing the elemental
628 distribution of different elements. (For interpretation of the references to color in this
629 figure legend, the reader is referred to the web version of this article).

630